

Constraints on Sub-GeV Dark Matter-Electron Scattering from the DarkSide-50 Experiment

P. Agnes,¹ I. F. M. Albuquerque,² T. Alexander,³ A. K. Alton,⁴ G. R. Araujo,² D. M. Asner,⁵ M. P. Ave,² H. O. Back,³ B. Baldin,⁶ G. Batignani,^{7,8} K. Biery,⁶ V. Bocci,⁹ G. Bonfini,¹⁰ W. Bonivento,¹¹ B. Bottino,^{12,13} F. Budano,^{14,15} S. Bussino,^{14,15} M. Cadeddu,^{16,11} M. Cadoni,^{16,11} F. Calaprice,¹⁷ A. Caminata,¹³ N. Canci,^{1,10} A. Candela,¹⁰ M. Caravati,^{16,11} M. Cariello,¹³ M. Carlini,¹⁰ M. Carpinelli,^{18,19} S. Catalanotti,^{20,21} V. Cataudella,^{20,21} P. Cavalcante,^{22,10} S. Cavuoti,^{20,21} A. Chepurinov,²³ C. Cicalò,¹¹ L. Cifarelli,^{24,25} A. G. Cocco,²¹ G. Covone,^{20,21} D. D'Angelo,^{26,27} M. D'Incecco,¹⁰ D. D'Urso,^{18,19} S. Davini,¹³ A. De Candia,^{20,21} S. De Cecco,^{9,28} M. De Deo,¹⁰ G. De Filippis,^{20,21} G. De Rosa,^{20,21} M. De Vincenzi,^{14,15} P. Demontis,^{18,19,29} A. V. Derbin,³⁰ A. Devoto,^{16,11} F. Di Eusanio,¹⁷ G. Di Pietro,^{10,27} C. Dionisi,^{9,28} M. Downing,³¹ E. Edkins,³² A. Empl,¹ A. Fan,³³ G. Fiorillo,^{20,21} K. Fomenko,³⁴ D. Franco,³⁵ F. Gabriele,¹⁰ A. Gabrieli,^{18,19} C. Galbiati,^{17,27} P. Garcia Abia,³⁶ S. Giagu,^{9,28} C. Giganti,³⁷ G. K. Giovanetti,¹⁷ O. Gorchakov,³⁴ A. M. Goretta,¹⁰ F. Granato,³⁸ M. Gromov,²³ M. Guan,³⁹ Y. Guardincerri,^{6, a} M. Gulino,^{40,19} B. R. Hackett,³² M. H. Hassanshahi,¹⁰ K. Herner,⁶ B. Hosseini,¹¹ D. Hughes,¹⁷ P. Humble,³ E. V. Hungerford,¹ Al. Ianni,¹⁰ An. Ianni,^{17,10} V. Ippolito,⁹ I. James,^{14,15} T. N. Johnson,⁴¹ Y. Kahn,¹⁷ K. Keeter,⁴² C. L. Kendziora,⁶ I. Kochanek,¹⁷ G. Koh,¹⁷ D. Korablev,³⁴ G. Korga,^{1,10} A. Kubankin,⁴³ M. Kuss,⁷ M. La Commara,^{20,21} M. Lai,^{16,11} X. Li,¹⁷ M. Lisanti,¹⁷ M. Lissia,¹¹ B. Loer,³ G. Longo,^{20,21} Y. Ma,³⁹ A. A. Machado,⁴⁴ I. N. Machulin,^{45,46} A. Mandarano,^{47,10} L. Mapelli,¹⁷ S. M. Mari,^{14,15} J. Maricic,³² C. J. Martoff,³⁸ A. Messina,^{9,28} P. D. Meyers,¹⁷ R. Milincic,³² S. Mishra-Sharma,¹⁷ A. Monte,³¹ M. Morrocchi,⁷ B. J. Mount,⁴² V. N. Muratova,³⁰ P. Musico,¹³ R. Nania,²⁵ A. Navrer Agasson,³⁷ A. O. Nozdrina,^{45,46} A. Oleinik,⁴³ M. Orsini,¹⁰ F. Ortica,^{48,49} L. Pagani,⁴¹ M. Pallavicini,^{12,13} L. Pandola,¹⁹ E. Pantic,⁴¹ E. Paoloni,^{7,8} F. Pazzona,^{18,19} K. Pelczar,¹⁰ N. Pelliccia,^{48,49} V. Pesudo,³⁶ A. Pocar,³¹ S. Pordes,⁶ S. S. Poudel,¹ D. A. Pugachev,⁴⁵ H. Qian,¹⁷ F. Ragusa,^{26,27} M. Razeti,¹¹ A. Razeto,¹⁰ B. Reinhold,³² A. L. Renshaw,¹ M. Rescigno,⁹ A. Romani,^{48,49} B. Rossi,²¹ N. Rossi,⁹ D. Sablone,^{17,10} O. Samoylov,³⁴ W. Sands,¹⁷ S. Sanfilippo,^{15,14} M. Sant,^{18,19} R. Santorelli,³⁶ C. Savarese,^{47,10} E. Scapparone,²⁵ B. Schlitzer,⁴¹ E. Segreto,⁴⁴ D. A. Semenov,³⁰ A. Shchagin,⁴³ A. Sheshukov,³⁴ P. N. Singh,¹ M. D. Skorokhvatov,^{45,46} O. Smirnov,³⁴ A. Sotnikov,³⁴ C. Stanford,¹⁷ S. Stracka,⁷ G. B. Suffritti,^{18,19,29} Y. Suvorov,^{20,21,33,45} R. Tartaglia,¹⁰ G. Testera,¹³ A. Tonazzo,³⁵ P. Trinchese,^{20,21} E. V. Unzhakov,³⁰ M. Verducci,^{9,28} A. Vishneva,³⁴ B. Vogelaar,²² M. Wada,¹⁷ T. J. Waldrop,⁴ H. Wang,³³ Y. Wang,³³ A. W. Watson,³⁸ S. Westerdale,^{17, b} M. M. Wojcik,⁵⁰ M. Wojcik,⁵¹ X. Xiang,¹⁷ X. Xiao,³³ C. Yang,³⁹ Z. Ye,¹ C. Zhu,¹⁷ A. Zichichi,^{24,25} and G. Zuzel⁵⁰

¹Department of Physics, University of Houston, Houston, TX 77204, USA

²Instituto de Física, Universidade de São Paulo, São Paulo 05508-090, Brazil

³Pacific Northwest National Laboratory, Richland, WA 99352, USA

⁴Physics Department, Augustana University, Sioux Falls, SD 57197, USA

⁵Brookhaven National Laboratory, Upton, NY 11973, USA

⁶Fermi National Accelerator Laboratory, Batavia, IL 60510, USA

⁷INFN Pisa, Pisa 56127, Italy

⁸Physics Department, Università degli Studi di Pisa, Pisa 56127, Italy

⁹INFN Sezione di Roma, Roma 00185, Italy

¹⁰INFN Laboratori Nazionali del Gran Sasso, Assergi (AQ) 67100, Italy

¹¹INFN Cagliari, Cagliari 09042, Italy

¹²Physics Department, Università degli Studi di Genova, Genova 16146, Italy

¹³INFN Genova, Genova 16146, Italy

¹⁴INFN Roma Tre, Roma 00146, Italy

¹⁵Mathematics and Physics Department, Università degli Studi Roma Tre, Roma 00146, Italy

¹⁶Physics Department, Università degli Studi di Cagliari, Cagliari 09042, Italy

¹⁷Physics Department, Princeton University, Princeton, NJ 08544, USA

¹⁸Chemistry and Pharmacy Department, Università degli Studi di Sassari, Sassari 07100, Italy

¹⁹INFN Laboratori Nazionali del Sud, Catania 95123, Italy

²⁰Physics Department, Università degli Studi "Federico II" di Napoli, Napoli 80126, Italy

²¹INFN Napoli, Napoli 80126, Italy

- ²² *Virginia Tech, Blacksburg, VA 24061, USA*
- ²³ *Skobeltsyn Institute of Nuclear Physics, Lomonosov Moscow State University, Moscow 119991, Russia*
- ²⁴ *Physics Department, Università degli Studi di Bologna, Bologna 40126, Italy*
- ²⁵ *INFN Bologna, Bologna 40126, Italy*
- ²⁶ *Physics Department, Università degli Studi di Milano, Milano 20133, Italy*
- ²⁷ *INFN Milano, Milano 20133, Italy*
- ²⁸ *Physics Department, Sapienza Università di Roma, Roma 00185, Italy*
- ²⁹ *Interuniversity Consortium for Science and Technology of Materials, Firenze 50121, Italy*
- ³⁰ *Saint Petersburg Nuclear Physics Institute, Gatchina 188350, Russia*
- ³¹ *Amherst Center for Fundamental Interactions and Physics
Department, University of Massachusetts, Amherst, MA 01003, USA*
- ³² *Department of Physics and Astronomy, University of Hawai'i, Honolulu, HI 96822, USA*
- ³³ *Physics and Astronomy Department, University of California, Los Angeles, CA 90095, USA*
- ³⁴ *Joint Institute for Nuclear Research, Dubna 141980, Russia*
- ³⁵ *APC, Université Paris Diderot, CNRS/IN2P3, CEA/Irfu, Obs de Paris, USPC, Paris 75205, France*
- ³⁶ *CIEMAT, Centro de Investigaciones Energéticas, Medioambientales y Tecnológicas, Madrid 28040, Spain*
- ³⁷ *LPNHE, CNRS/IN2P3, Sorbonne Université, Université Paris Diderot, Paris 75252, France*
- ³⁸ *Physics Department, Temple University, Philadelphia, PA 19122, USA*
- ³⁹ *Institute of High Energy Physics, Beijing 100049, China*
- ⁴⁰ *Engineering and Architecture Faculty, Università di Enna Kore, Enna 94100, Italy*
- ⁴¹ *Department of Physics, University of California, Davis, CA 95616, USA*
- ⁴² *School of Natural Sciences, Black Hills State University, Spearfish, SD 57799, USA*
- ⁴³ *Radiation Physics Laboratory, Belgorod National Research University, Belgorod 308007, Russia*
- ⁴⁴ *Physics Institute, Universidade Estadual de Campinas, Campinas 13083, Brazil*
- ⁴⁵ *National Research Centre Kurchatov Institute, Moscow 123182, Russia*
- ⁴⁶ *National Research Nuclear University MEPhI, Moscow 115409, Russia*
- ⁴⁷ *Gran Sasso Science Institute, L'Aquila 67100, Italy*
- ⁴⁸ *Chemistry, Biology and Biotechnology Department, Università degli Studi di Perugia, Perugia 06123, Italy*
- ⁴⁹ *INFN Perugia, Perugia 06123, Italy*
- ⁵⁰ *M. Smoluchowski Institute of Physics, Jagiellonian University, 30-348 Krakow, Poland*
- ⁵¹ *Department of Chemistry, Lodz University of Technology, 93-590 Lodz, Poland*
- (Dated: December 3, 2024)

We present new constraints on sub-GeV dark matter particles scattering off electrons in argon based on an analysis of ionization signal data from the DarkSide-50 detector.

The analysis presented here follows directly from the analysis done in Ref. [1], a search for sub-10 GeV/ c^2 WIMPs using ionization signals from the DarkSide-50 detector. We refer the reader to Ref. [1] for a discussion of the DarkSide-50 apparatus, data selection, detector response, and trigger and cut efficiencies.

The nature of dark matter (DM) remains unknown despite several decades of increasingly compelling gravitational evidence [2–6]. While the most favored candidate in a particle physics interpretation is the Weakly Interacting Massive Particle (WIMP) [7, 8], which obtains its relic abundance by thermal freeze-out through weak interactions, there is as yet no unambiguous evidence of WIMP direct detection.

Another well-motivated class of DM candidates is sub-GeV particles interacting through a light mediator with couplings smaller than the weak-scale. These light DM candidates arise in a variety of models [9–14] and can be fixed through a number of mechanisms to obtain the correct DM abundance [15–20]. Sub-GeV DM will generically have

couplings to electrons. Because the energy transferred to the target particle depends on the reduced mass of the system, electron targets can more efficiently absorb the kinetic energy for DM below the GeV scale compared to nuclear targets [21]. There is currently a substantial experimental effort to search for sub-GeV DM through multiple techniques [22–27]. In particular, dual-phase noble liquid detectors are an excellent probe of sub-GeV DM, which can ionize electrons to create a scintillation signal (S2) even when the corresponding prompt scintillation signal (S1), typically used to identify nuclear recoils, is below the detector threshold [28]. Indeed, even if sub-GeV DM interacted with nuclei, the nuclear recoil signal would be difficult to detect because of the unfavorable mass ratio between DM and target. In this note, we present the first limits on sub-GeV DM-electron scattering from the DarkSide-50 experiment.

We evaluate the dark matter recoil spectra for argon following the calculation of Refs. [21, 30]. The

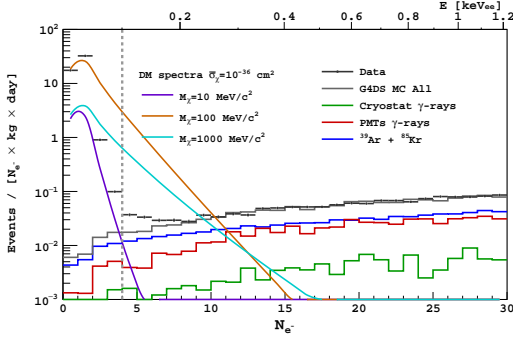


FIG. 1. The 500 d DarkSide-50 ionization spectrum compared with predicted spectra from the G4DS background simulation[29]. Also shown are calculated DM-electron scattering spectra for DM particles with masses of 10, 100, and 1000 MeV/c², reference cross section of 10⁻³⁶ cm², and $|F_{\text{DM}}(q)|^2 = 1$. The vertical dashed line indicates the $N_{e^-} = 4$ analysis threshold.

DM-electron differential scattering rate is given by

$$\frac{dR}{d \ln E_{\text{er}}} = N_T \frac{\rho_\chi}{m_\chi} \frac{\bar{\sigma}_e}{8 \mu_{\chi e}^2} \times \sum_{nl} \int dq q |f_{\text{ion}}^{nl}(k', q)|^2 |F_{\text{DM}}(q)|^2 \eta(v_{\text{min}}), \quad (1)$$

where N_T is the number of target atoms, $\rho_\chi = 0.3 \text{ GeV/cm}^3$ is the local DM density, m_χ is the DM mass, $\bar{\sigma}_e$ is the DM-electron reference cross section, $\mu_{\chi e}$ is the DM-electron reduced mass, n, l are the atomic orbital indices, q is the 3-momentum transfer, k' is the electron recoil momentum, v_{min} is the minimum DM speed, $\eta(v_{\text{min}})$ is the inverse mean speed, $|f_{\text{ion}}^{nl}(k', q)|^2$ is the ionization form factor, and $|F_{\text{DM}}(q)|^2$ is the DM form factor.

The DM form factor parametrizes the fundamental DM-electron interaction and has the following limiting values:

$$|F_{\text{DM}}(q)|^2 = \begin{cases} 1, & m_{\text{med}} \gg \alpha m_e \\ (\alpha m_e / q)^4, & m_{\text{med}} \ll \alpha m_e, \end{cases} \quad (2)$$

where m_e is the electron mass and α is the fine-structure constant. The first case corresponds to the ‘‘heavy mediator’’ regime, where the mass of the particle mediating the DM-electron interaction, m_{med} , is much larger than the typical momentum scale, chosen here to be $q_0 = \alpha m_e = 1/a_0$, where a_0 is the Bohr radius. The second case corresponds to the ‘‘light mediator’’ regime. Because $F_{\text{DM}}(q)$ is dimensionless by definition, the form factor for the light mediator regime needs to be defined with respect to a reference momentum scale; αm_e is the conventional choice because this is typical of atomic momenta.

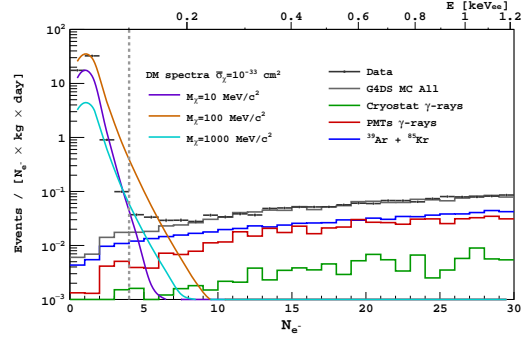


FIG. 2. The 500 d DarkSide-50 ionization spectrum compared with predicted spectra from the G4DS background simulation[29]. Also shown are calculated DM-electron scattering spectra for DM particles with masses of 10, 100, and 1000 MeV/c², reference cross section of 10⁻³³ cm², and $|F_{\text{DM}}(q)|^2 = (\alpha m_e / q)^4$. The vertical dashed line indicates the $N_{e^-} = 4$ analysis threshold.

The inverse mean speed, $\eta(v_{\text{min}})$, is defined through the DM velocity distribution in exactly the same way as for GeV-scale WIMPs and nuclear scattering. We have assumed the Standard Halo Model with escape velocity $v_{\text{esc}} = 544 \text{ km/s}$, circular velocity $v_0 = 220 \text{ km/s}$, and the Earth velocity as specified in [31] and evaluated at $t = 199$ days ($v_E \approx 244 \text{ km/s}$), the median run live-time time for DarkSide-50. Note that the definition of v_{min} is different for electron scattering from a bound initial state:

$$v_{\text{min}} = \frac{|E_b^{nl}| + E_{\text{er}}}{q} + \frac{q}{2m_\chi}. \quad (3)$$

The numerator of the first term is the total energy transferred to the ionized electron, which is a sum of the (positive) binding energy, E_b^{nl} , in the atomic orbital with principal quantum number n and angular momentum quantum number l , and the recoil energy of the outgoing electron.

The scattering rate for a DM particle interacting with an electron in an atom depends on the initial and final-state wavefunction of the electron. This requires one to model both the bound and continuum states of the electron. The target electron is parametrized by the Roothaan-Hartree-Fock wavefunctions for argon. The recoil electron wavefunction is the full positive-energy wavefunction obtained by solving the Schrödinger equation with a hydrogenic potential of some effective screened charge Z_{eff} [32]. We choose a Z_{eff} that reproduces the true energy of the argon bound-state wave function, assuming a pure Coulomb potential. Further details on this matching procedure are provided in the Appendix.

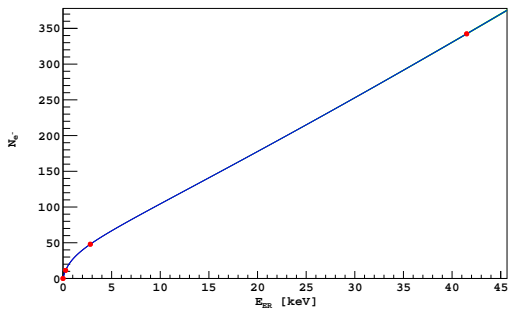


FIG. 3. Polynomial fit (blue) to the mean N_{e^-} measured for several peaks of known energy: the 2.82 keV K-shell and 0.27 keV L-shell lines from the electron capture of ^{37}Ar and the 41.5 keV peak from the decay of a ^{83m}Kr source. The polynomial is constrained to intersect the origin. The uncertainty of the fit is shown by the green band.

In the literature, different procedures have been used to approximate the outgoing electron wavefunction in such scattering scenarios. One common approximation is to treat the final state as a pure plane wave corrected by a Fermi factor,

$$F(k', Z_{\text{eff}}) = \frac{2\pi Z_{\text{eff}}}{k' a_0} \frac{1}{1 - e^{-2\pi Z_{\text{eff}}/(k' a_0)}}, \quad (4)$$

which parameterizes the distortion of the outgoing electron wavefunction by the effective screened Coulomb potential of the nucleus. While the approximate shape of the ionization form factors, f_{ion}^{nl} , are consistent between the plane-wave and full-continuum solutions, the detailed structure does vary between the two. At large momentum transfers, the plane-wave and continuum solutions approach each other, but they diverge at lower momentum transfers where the form factor is dominated by the overlap between the bound and continuum wavefunctions near the origin. The reason for this is that the Fermi factor reproduces the behavior of the full wavefunction at the origin, but outer-shell orbitals have most of their support away from the origin, such that the overlap with the outgoing wavefunction is maximized away from the origin. Thus, smaller atoms and inner shells have better agreement. For this reason, the discrepancy between using continuum versus plane-wave final states is smaller for argon than for xenon. We however choose to use the full-continuum solutions for the presentation of all final results in this work.

The calculated DM-electron recoil spectra are converted to ionization spectra based on a fit to several low energy electron recoil peaks of known energy, as shown in Fig 3 and described in [1]. The resulting ionization spectra are then smeared assum-

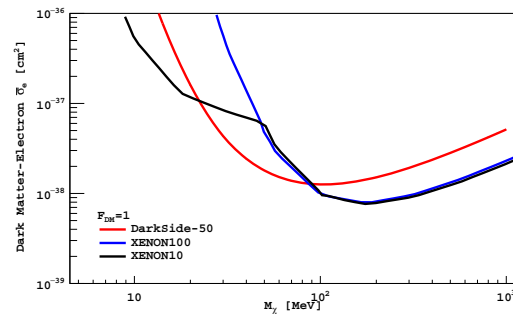


FIG. 4. 90% C.L. limits on the DM-electron scattering cross section for $F_{\text{DM}} = 1$ for DarkSide-50 (red) alongside limits calculated in [30] using data from XENON10 (black) and XENON100 (blue).

ing the ionization yield and recombination processes follow a binomial distribution and convolved with the detector response, measured from single-electron events [1]. This procedure correctly reconstructs the measured width of the ^{37}Ar K-shell (2.82 keV) and L-shell (0.27 keV) peaks. The expected DM-electron scattering ionization spectra in the case of a heavy mediator are shown in Fig. 1 and in the case of a light mediator in Fig. 2.

We use a 500 day dataset collected between April 30, 2015, and April 25, 2017, corresponding to a 6786.0 kg d exposure, to place limits on sub-GeV DM. Details on data selection, cut efficiencies, and electron recoil energy calibration can be found in [1]. The 500 day ionization spectrum used for the search is shown in Fig. 1. Limits are calculated using a binned profile likelihood method implemented in RooStats [33–35]. We use an analysis threshold of $N_{e^-} = 4$, equivalent to 0.1 keVee. In this energy region, the hardware trigger efficiency is 100%. The background model used in the analysis is determined by a detailed Monte Carlo simulation of the DarkSide-50 apparatus. Spectral features at high energy are used to constrain the simulated radiological activity within detector components to predict the background spectrum in the region of interest. The predicted spectrum is plotted alongside the data in Fig. 1 and described in greater detail in [1]. During the analysis, the overall normalization of the background model is constrained near its predicted value by a Gaussian nuisance term in the likelihood function. Additional gaussian constraints on the background and signal spectral shape are included based on the uncertainty of the fit in Fig. 3 and the uncertainty in the S2 to N_{e^-} conversion factor, extracted from single-electron data.

The resulting 90% C.L. limits are shown in Fig. 4 and Fig. 5 for two assumptions of DM form-factors,

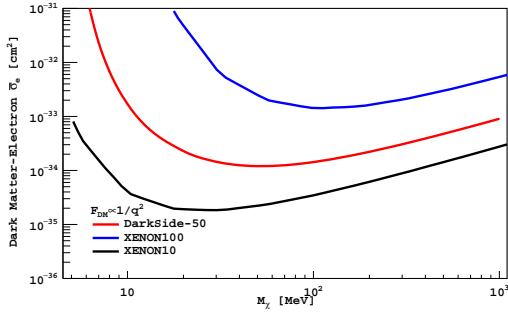


FIG. 5. 90% C.L. limits on the DM-electron scattering cross section for $F_{\text{DM}} \propto 1/q^2$ from DarkSide-50 (red) alongside limits calculated in [30] using data from XENON10 (black) and XENON100 (blue).

$F_{\text{DM}} = 1$ and $|F_{\text{DM}}(q)|^2 = (\alpha m_e/q)^4$. In the case of a heavy mediator, $F_{\text{DM}} = 1$, we improve the exclusion limit in the range from $30 \text{ MeV}/c^2$ to $70 \text{ MeV}/c^2$ over existing limits from XENON10 and XENON100 [30]. For $F_{\text{DM}} \propto 1/q^2$, our cross-section bound is limited by the $N_{e^-} - 4$ analysis threshold.

The DarkSide Collaboration offers its profound gratitude to the LNGS and its staff for their invaluable technical and logistical support. We also thank the Fermilab Particle Physics, Scientific, and Core Computing Divisions. Construction and operation of the DarkSide-50 detector was supported by the U.S. National Science Foundation (NSF) (Grants PHY-0919363, PHY-1004072, PHY-1004054, PHY-1242585, PHY-1314483, PHY-1314501, PHY-1314507, PHY-1352795, PHY-1622415, and associated collaborative grants PHY-1211308 and PHY-1455351), the Italian Istituto Nazionale di Fisica Nucleare, the U.S. Department of Energy (Contracts DE-FG02-91ER40671, DE-AC02-07CH11359, and DE-AC05-76RL01830), the Russian Science Foundation (Grant 16-12-10369), the Polish NCN (Grant UMO-2014/15/B/ST2/02561) and the Foundation for Polish Science (Grant Team2016-2/17). We also acknowledge financial support from the French Institut National de Physique Nucléaire et de Physique des Particules (IN2P3), from the UnivEarthS Labex program of Sorbonne Paris Cité (Grants ANR-10-LABX-0023 and ANR-11-IDEX-0005-02), and from the São Paulo Research Foundation (FAPESP) (Grant 2016/09084-0).

^a Deceased.

^b Currently at Carleton University, Ottawa, Canada.

[1] P. Agnes et al., [arXiv:Low-mass Dark Matter Search with the DarkSide-50 Experiment \(2018\)](#).

- [2] S. M. Faber and J. S. Gallagher, *Annu. Rev. Astro. Astrophys.* **17**, 135 (1979).
- [3] A. Refregier, *Annu. Rev. Astro. Astrophys.* **41**, 645 (2003).
- [4] D. Clowe et al., *Ap. J.* **648**, L109 (2006).
- [5] R. Thompson, R. Davé, and K. Nagamine, *Month. Not. Royal Astron. Soc.* **452**, 3030 (2015).
- [6] P. A. R. Ade et al. (The Planck Collaboration), *Astro. & Ap.* **594**, A13 (2016).
- [7] G. Steigman and M. S. Turner, *Nucl. Phys. B* **253**, 375 (1985).
- [8] G. Bertone, D. Hooper, and J. Silk, *Phys. Rep.* **405**, 279 (2005).
- [9] C. Boehm and P. Fayet, *Nuclear Physics B* **683**, 219 (2004).
- [10] M. J. Strassler and K. M. Zurek, *Physics Letters B* **651**, 374 (2007).
- [11] D. Hooper and K. M. Zurek, *Phys. Rev. D* **77**, 087302 (2008).
- [12] M. Pospelov, A. Ritz, and M. Voloshin, *Physics Letters B* **662**, 53 (2008).
- [13] J. L. Feng and J. Kumar, *Phys. Rev. Lett.* **101**, 231301 (2008).
- [14] R. Foadi, M. T. Frandsen, and F. Sannino, *Phys. Rev. D* **80**, 037702 (2009).
- [15] K. Petraki and R. R. Volkas, *International Journal of Modern Physics A* **28**, 1330028 (2013).
- [16] N. Bernal et al., *International Journal of Modern Physics A* **32**, 1730023 (2017).
- [17] Y. Hochberg et al., *Phys. Rev. Lett.* **115**, 021301 (2015).
- [18] R. T. D’Agnolo and J. T. Ruderman, *Phys. Rev. Lett.* **115**, 061301 (2015).
- [19] E. Kuflik, M. Perelstein, N. R.-L. Lorier, and Y.-D. Tsai, *Phys. Rev. Lett.* **116**, 221302 (2016).
- [20] E. Kuflik, M. Perelstein, N. R.-L. Lorier, and Y.-D. Tsai, *Journal of High Energy Physics* **2017**, 78 (2017).
- [21] R. Essig, J. Mardon, and T. Volansky, *Phys. Rev. D* **85**, 076007 (2012).
- [22] P. W. Graham, D. E. Kaplan, S. Rajendran, and M. T. Walters, *Physics of the Dark Universe* **1**, 32 (2012).
- [23] R. Essig et al., [arXiv:1311.0029 \(2013\)](#).
- [24] S. K. Lee, M. Lisanti, S. Mishra-Sharma, and B. R. Safdi, [arXiv p. 129 \(2015\)](#).
- [25] Y. Hochberg et al., [arXiv:1606.08849v2 \(2016\)](#).
- [26] M. Battaglieri et al., [arXiv:1707.04591v1 \(2017\)](#).
- [27] S. Derenzo et al., *Phys. Rev. D* **96**, 016026 (2017).
- [28] R. Essig et al., *Phys. Rev. Lett.* **109**, 860 (2012).
- [29] P. Agnes et al. (The DarkSide Collaboration), *JINST* **12**, P10015 (2017).
- [30] R. Essig, T. Volansky, and T.-T. Yu, *Phys. Rev. D* **96**, 043017 (2017).
- [31] S. K. Lee, M. Lisanti, and B. R. Safdi, *JCAP* **2013**, 033 (2013).
- [32] H. Bethe and E. Salpeter, *Quantum Mechanics of One- and Two-Electron Atoms*, Springer Berlin Heidelberg (2013), ISBN 9783662128695.
- [33] G. Cowan, K. Cranmer, E. Gross, and O. Vitells, *Eur. Phys. J. C* **71**, 1 (2011).

- [34] L. Moneta et al., [PoSACAT2010](#), 057:1009.1003 (2010).
- [35] W. Verkerke and D. P. Kirkby, [eConfC0303241](#), [MOLT007:physics/0306116](#) (2003), [186(2003)].
- [36] C. F. Bunge, J. A. Barrientos, and A. V. Bunge, [Atomic Data and Nuclear Data Tables](#) **53**, 113 (1993).

APPENDIX

Here we provide additional details on the DM-electron scattering rate calculation described in the text. The explicit forms of the radial part of ψ_{nl} used to compute the atomic form factor, $|f_{\text{ion}}^{nl}(k', q)|^2$, are given by the Roothaan-Hartree-Fock (RHF) wavefunctions [36], which are linear combinations of Slater-type orbitals:

$$R_{nl}(r) = a_0^{-3/2} \sum_j C_{jln} \frac{(2Z_{jl})^{n'_{jl}+1/2}}{\sqrt{(2n'_{jl})!}} \times \left(\frac{r}{a_0}\right)^{n'_{jl}-1} e^{-Z_{jl}r/a_0}. \quad (\text{A.5})$$

The continuum-state solutions to the Schrödinger equation with potential $-Z_{\text{eff}}/r$ have radial wavefunctions indexed by l and k , given by [32]

$$\tilde{R}_{kl}(r) = (2\pi)^{3/2} \frac{\sqrt{\frac{2}{\pi}} \left| \Gamma\left(l+1 + \frac{iZ_{\text{eff}}}{ka_0}\right) \right| e^{\frac{\pi Z_{\text{eff}}}{2ka_0}}}{(2l+1)!} \times e^{ikr} {}_1F_1\left(l+1 + \frac{iZ_{\text{eff}}}{ka_0}, 2l+2, 2ikr\right). \quad (\text{A.6})$$

The ratio of the wavefunction at the origin to the wavefunction at infinity gives the Fermi factor:

$$\left| \frac{\tilde{R}_{kl}(r=0)}{\tilde{R}_{kl}(r=\infty)} \right|^2 = F(k, Z_{\text{eff}}). \quad (\text{A.7})$$

The normalization for these unbound wavefunctions is

$$\int dr r^2 \tilde{R}_{kl}^*(r) R_{k'l'}(r) = (2\pi)^3 \frac{1}{k^2} \delta_{ll'} \delta(k-k'), \quad (\text{A.8})$$

so that $\tilde{R}_{kl}(r)$ itself is dimensionless. In terms of these wavefunctions, the ionization form factor is given by

$$|f_{\text{ion}}^{nl}(k', q)|^2 = \frac{4k'^3}{(2\pi)^3} \sum_{l'} \sum_{L=|l'-l|}^{l'+l} (2l+1)(2l'+1) \times \left[\begin{matrix} l & l' & L \\ 0 & 0 & 0 \end{matrix} \right]^2 \left| \int dr r^2 \tilde{R}_{k'l'}(r) R_{nl}(r) j_L(qr) \right|^2 \quad (\text{A.9})$$

The term in brackets is the Wigner- $3j$ symbol evaluated at $m_1 = m_2 = m_3 = 0$, and j_L is the spherical Bessel function of order L . With the given normalizations, the integral has dimension $3/2$, so the mod-squared has dimension 3, resulting in a dimensionless $|f_{\text{ion}}^{nl}(k', q)|^2$ as required.

Following [28, 30], the procedure used to determine Z_{eff} is:

1. Treat the bound-state orbital R_{nl} as a bound state of a pure Coulomb potential $-Z_{\text{eff}}^{nl}/r$, rather than the self-consistent potential giving rise to the RHF wavefunctions.
2. Determine Z_{eff}^{nl} by matching the energy eigenvalue to the RHF eigenvalue.
3. Use this Z_{eff}^{nl} to construct all $\tilde{R}_{k'l'}(r)$ in the sum in Eq. (A.9).

For example, for the $3p$ shell of argon, $E_b^{3p} = 16.08$ eV, so we solve

$$13.6 \text{ eV} \times \frac{(Z_{\text{eff}}^{3p})^2}{3^2} = 16.08 \text{ eV} \implies Z_{\text{eff}}^{3p} = 3.26.$$